INTERNATIONAL JOURNAL OF ROBUST AND NONLINEAR CONTROL
Int. J. Robust Nonlinear Control 2015; **25**:791–808
Published online 3 December 2013 in Wiley Online Library (wileyonlinelibrary.com). DOI: 10.1002/rnc.3104

Design of the multi-objective constrained nonlinear robust excitation controller with extended Kalman filter estimates of all state variables

Gu Zhifeng[1,*,†], Yang Guixin[2], Zhu Changqing[1] and Shao Tianzhang[1]

[1] *Vehicles and Electrical Department, Mechanical Engineering College, Shi Jiazhuang 050003, China*
[2] *54th Research Institute, China Electronics Technology Corporation, Shi Jiazhuang 050081, China*

SUMMARY

A new optimal back-stepping robust adaptive control method for the military moving power station (MMPS) excitation system is proposed in this paper. Through the extended Kalman filter estimates of the state variables, the tracking of the operating point, and the back-stepping technique, the proposed controller has been shown to improve system robustness to disturbances and dynamic uncertainties and minimise the effect of disturbances by solving the linear matrix inequality to obtain the optimal control law on all operating points. The simulation and experimental results show that the proposed control strategy can enhance the transient stability of the MMPS excitation system more effectively than other methods and can optimise the convergence rates of the state variables by modifying the values of the weighting matrices. Moreover, the terminal voltage of the MMPS can be sampled quickly by alternating current (AC) tracking comparison. Copyright © 2013 John Wiley & Sons, Ltd.

Received 19 December 2012; Revised 10 October 2013; Accepted 12 October 2013

KEY WORDS: optimal back-stepping design; optimal robust adaptive excitation control; optimal L2 gain disturbance attenuation; EKF estimates; AC tracking excitation; military moving power station

1. INTRODUCTION

The electrical network capacity of a large ship or a military moving power station (MMPS) is limited compared with that of the civil infinite power system. The instantaneity and randomness of the weapon equipment, such as artillery and radar, can easily affect this electrical network. Thus, excitation controller design has attracted considerable attention as an effective and economical method to improve the dynamic performance and stability of electrical networks [1–6].

Several kinds of excitation systems (such as the phase compound excitation system and the harmonic excitation system) are used in the ship power station (SPS) and the MMPS. However, the PID excitation control method is usually adopted. The excitation system possesses nonlinearity. Thus, the traditional PID control method cannot provide satisfactory performance. Advanced nonlinear control methods have recently been used in excitation control, such as exact feedback linearisation [7–9], intelligent control method [10, 11], direct feedback linearisation method [12, 13], Hamilton [14, 15], sliding mode control [16] and nonlinear robust control [17].

Robust adaptive excitation control (RAEC) has attracted considerable attention because of the numerous disturbances and uncertain parameters in the excitation system, such as electromagnetic interference, torque interference, and immeasurable damping coefficient [18–23]. The RAEC, using dynamic estimates of unknown parameters, is more appropriate for solving unknown-parameter

*Correspondence to: Gu Zhifeng, Vehicles and Electrical Department, Mechanical Engineering College, Shi Jiazhuang 050003, China.
†E-mail: gzfjxxy@163.com

problems. However, the controller is usually designed on the given operating point, and optimal control is not considered in RAEC. The excitation control of the MMPS on all operating points is required because of the random variation of loads. The bus voltage in the civil infinite power system is constant, but the electrical network voltage of the SPS or the MMPS is easily affected by load variation. Thus, in the RAEC of the SPS or the MMPS, the generator terminal voltage should be rapidly sampled, and the sampling speed will affect the control speed.

Motivated by the aforementioned observation, the AC tracking optimal back-stepping robust adaptive control (OBRAC) is presented and applied to the excitation control of MMPS in this study. In the OBRAC method, the controller can adapt to uncertain parameters, is robust to disturbances and can be applied to minimise the effect of disturbances by solving the LMI to obtain the optimal control law against the worst disturbances. Optimal back-stepping robust adaptive excitation control (OBRAEC) is a type of state feedback control technique that requires the values of the state variables to be known. In this paper, the state variables of the excitation system on different operating points are estimated by the extended Kalman filter (EKF) and then calculated synchronously. In the calculation of the state variables, the terminal voltage of the MMPS is obtained through AC tracking comparison.

The remainder of this paper is organised as follows. The excitation system model of the MMPS is established in Section 2. Section 3 discusses the state EKF estimation and the AC tracking voltage sampling method. Section 4 presents the OBRAEC design. Section 5 includes the simulation and experiment results. The conclusions are summarised in Section 6.

2. MATHEMATICAL MODEL OF THE EXCITATION SYSTEM AND CONTROL ANALYSIS

The excitation system of the MMPS, with uncertain parameters and disturbances, can be expressed by the following third-order model [12]:

$$
\begin{aligned}
\dot{\delta} &= \omega - \omega_0 \\
\dot{\omega} &= -\frac{D}{2H}(\omega - \omega_0) - \frac{\omega_0}{2H}(P_e - P_m) + \varepsilon_1 \\
\dot{E}'_q &= -\frac{1}{T'_q}E'_q + \frac{x_{\mathrm{d}} - x'_{\mathrm{d}}}{T_{\mathrm{d}0}x_{\mathrm{d}}}u_{\mathrm{s}}\cos\delta + \frac{1}{T_{\mathrm{d}0}}V_f + \varepsilon_2
\end{aligned}
$$

where δ is the power angle, ω is the rotor speed of the generator, P_m is the mechanical input power, P_e is the active electrical power, H is the inertia constant, D is the damping constant, $T'_{\mathrm{d}} = T_{\mathrm{d}0}\frac{x'_{\mathrm{d}}}{x_{\mathrm{d}}}$ is the direct axis transient time constant, ε_i is the disturbance, V_f is the electromotive force (EMF) in the excitation coil of the generator, u_s is the terminal voltage of the MMPS and E'_q is the transient EMF in the orthogonal axis of the generator.

The coordinate transformation is defined as follows:

$$
x = \begin{bmatrix} x_1 & x_2 & x_3 \end{bmatrix}^{\mathrm{T}} = \begin{bmatrix} \delta - \delta_0 & \omega - \omega_0 & E'_q - E'_{q0} \end{bmatrix}^{\mathrm{T}} \text{ and } u = V_f - V_{f0}
$$

where $\begin{bmatrix} \delta_0 & \omega_0 & E'_{q0} & V_{f0} \end{bmatrix}$ is the given operating point of the generator. The output of the system is defined as $y_i = x_i - x_{i0}$. The control object is to drive the output y_i to a small neighbourhood of the origin.

In the new coordinate, the nonlinear generator model is given by

$$
\dot{x}_1 = x_2 \tag{1.1}
$$

$$
\dot{x}_2 = -\frac{D}{2H}x_2 - \beta_1 u_{\mathrm{s}}\sin(\delta_0 + x_1)x_3 - \beta_1 u_{\mathrm{s}} x_{30}\left[\sin(\delta_0 + x_1) - \sin(\delta_0)\right] + \varepsilon_1 \tag{1.2}
$$

$$
\dot{x}_3 = -\beta_2 x_3 - \beta_3 u_{\mathrm{s}}\left[\cos(\delta_0) - \cos(\delta_0 + x_1)\right] + \frac{1}{T_{\mathrm{d}0}}u + \varepsilon_2 \tag{1.3}
$$

where $\beta_1 = \frac{\omega_0}{2Hx_{\mathrm{d}}}$, $\beta_2 = \frac{1}{T'_{\mathrm{d}}}$, $\beta_3 = \frac{x_{\mathrm{d}} - x'_{\mathrm{d}}}{T_{\mathrm{d}0}x_{\mathrm{d}}}$.

D cannot be measured accurately and is the unknown parameter.

DOI: 10.1002/rnc

In System (1), u_s is obtained by the rectifier and filter circuit and often fluctuates when loads suddenly increase. The excitation control speed will be affected because of the large time constant of the rectifier and filter circuit. In this paper, u_s is obtained using the AC tracking and comparing method (introduced in Section 3). To stabilise System (1), the OBRAC is proposed (introduced in Section 4). OBRAC is a state feedback control method that requires the state variable values to be known. In this paper, the values of these state variables are calculated as follows:

Step 1: When the values of ω, $\bar{\theta}$, $\varphi_{\delta \mathrm{d}}$ and $\varphi_{\delta \mathrm{q}}$ are obtained by EKF (introduced in Section 3), δ, i_{d}, i_{q}, P_{e}, Q_{e} and φ can be calculated by

$$\delta = ar\tan\left(\frac{\varphi_{\delta \mathrm{d}}}{\varphi_{\delta \mathrm{q}}}\right), \quad \begin{bmatrix} i_{\mathrm{d}} \\ i_{\mathrm{q}} \end{bmatrix} = \begin{bmatrix} \cos\bar{\theta} & -\sin\bar{\theta} \\ \sin\bar{\theta} & \cos\bar{\theta} \end{bmatrix} \begin{bmatrix} i_{\mathrm{D}} \\ i_{\mathrm{Q}} \end{bmatrix}, \quad \begin{bmatrix} u_{\mathrm{d}} \\ u_{\mathrm{q}} \end{bmatrix}$$
$$= \begin{bmatrix} \cos\bar{\theta} & -\sin\bar{\theta} \\ \sin\bar{\theta} & \cos\bar{\theta} \end{bmatrix} \begin{bmatrix} u_{\mathrm{D}} \\ u_{\mathrm{Q}} \end{bmatrix}, \quad P_{\mathrm{e}} = u_{\mathrm{d}} i_{\mathrm{d}} + u_{\mathrm{q}} i_{\mathrm{q}},$$

$Q_{\mathrm{e}} = u_{\mathrm{d}} i_{\mathrm{q}} - u_{\mathrm{q}} i_{\mathrm{d}}$ and $\varphi = \mathrm{ar}\tan \frac{P_{\mathrm{e}}}{Q_{\mathrm{e}}}$, respectively.

$$\text{where} \begin{bmatrix} i_{\mathrm{D}} \\ i_{\mathrm{Q}} \end{bmatrix} = \sqrt{\frac{2}{3}} \begin{bmatrix} 1 & -\frac{1}{2} & -\frac{1}{2} \\ 0 & \frac{\sqrt{3}}{2} & -\frac{\sqrt{3}}{2} \end{bmatrix} \begin{bmatrix} i_{\mathrm{a}} \\ i_{\mathrm{b}} \\ i_{\mathrm{c}} \end{bmatrix}; \begin{bmatrix} u_{\mathrm{D}} \\ u_{\mathrm{Q}} \end{bmatrix}$$
$$= \sqrt{\frac{2}{3}} \begin{bmatrix} 1 & -\frac{1}{2} & -\frac{1}{2} \\ 0 & \frac{\sqrt{3}}{2} & -\frac{\sqrt{3}}{2} \end{bmatrix} \begin{bmatrix} u_{\mathrm{a}} \\ u_{\mathrm{b}} \\ u_{\mathrm{c}} \end{bmatrix}; i_{\mathrm{a}}, i_{\mathrm{b}}, i_{\mathrm{c}}, u_{\mathrm{a}}, u_{\mathrm{b}} \text{ and } u_{\mathrm{c}}$$

are the instantaneous voltage and current values of the generator; ω is the rotor speed; $\bar{\theta}$ is the rotor position; $\varphi_{\delta \mathrm{d}}$ and $\varphi_{\delta \mathrm{q}}$ are the d-q axis stator flux linkages, respectively; i_{d} and i_{q} are the d-q axis stator currents, respectively; Q_e is the reactive power and φ is the power factor angle.

Step 2: When u_s is obtained by AC tracking comparison (introduced in Section 3), we obtain the value of E_q' by substituting δ, i_{d}, P_{e} and u_s into $P_{\mathrm{e}} = \frac{E_{\mathrm{q}} u_{\mathrm{s}}}{x_{\mathrm{d}}} \sin\delta + \frac{u_{\mathrm{s}}^2 (x_{\mathrm{d}} - x_{\mathrm{q}})}{2 x_{\mathrm{d}} x_{\mathrm{q}}} \sin 2\delta$ and $E_q' = E_q - \left(x_d - x_d'\right) i_d$.

Step 3: When the terminal voltage root mean square (RMS) value of the generator is U, the current RMS value I, the direct axis current RMS value I_d , δ_0 and E_{q0} can be calculated by $I = \frac{P_{\mathrm{e}}}{3U\cos\varphi}$, $I_{\mathrm{d}} = I\sin(\varphi + \delta_0)$, $\delta_0 = arc\cos\frac{U\cos\varphi}{\sqrt{(U\cos\varphi)^2 + (U\sin\varphi + I x_{\mathrm{q}})^2}}$ and $E_{\mathrm{q}0} = U\cos\delta_0 + I_{\mathrm{d}} x_{\mathrm{d}}$, respectively.
By substituting E_{q0} into $E_{\mathrm{q}0}' = E_{\mathrm{q}0} - \left(x_{\mathrm{d}} - x_{\mathrm{d}}'\right) I_{\mathrm{d}}$, $E_{\mathrm{q}0}'$ can be obtained.

Step 4: Substituting ω, δ, E_q', ω_0 (represents the norm speed of the generator), δ_0 and E_{q0}' into $\begin{bmatrix} x_1 & x_2 & x_3 \end{bmatrix}^{\mathrm{T}} = \begin{bmatrix} \delta - \delta_0 & \omega - \omega_0 & E_q' - E_{q0}' \end{bmatrix}^{\mathrm{T}}$, we can obtain the value of the state vector $\boldsymbol{x} = \begin{bmatrix} x_1 & x_2 & x_3 \end{bmatrix}^{\mathrm{T}}$.

3. VOLTAGE SAMPLING BASED ON FLUX LINKAGE ESTIMATION AND AC TRACKING COMPARISON

3.1. Flux linkage estimation by extended Kalman filter

The relationship between the rotor speed ω and the rotor position $\bar{\theta}$ is given by

$$\dot{\bar{\theta}} = \omega. \tag{2}$$

The rotor speed can be assumed to be constant in the sampling period because of the high sampling frequency in the excitation control system, that is

$$\dot{\omega} = 0. \tag{3}$$

In the d, q reference coordinate system, the flux linkage equation of the synchronous generator can be described as

$$\dot{\varphi}_{\delta\mathrm{d}} = u_\mathrm{d} + Ri_\mathrm{d} + \omega\varphi_{\delta\mathrm{q}} \tag{4}$$

$$\dot{\varphi}_{\delta\mathrm{q}} = u_\mathrm{q} + Ri_\mathrm{q} - \omega\varphi_{\delta\mathrm{d}} \tag{5}$$

$$\varphi_{\delta\mathrm{q}} = \varphi_\mathrm{aq} = L_\mathrm{q} i_\mathrm{q} \tag{6}$$

$$\varphi_{\delta\mathrm{d}} = \varphi_\mathrm{ad} + \varphi_\mathrm{f} = L_\mathrm{d} i_\mathrm{d} + \varphi_\mathrm{f} \tag{7}$$

$$\dot{\varphi}_{\delta} = \dot{\varphi}_{\delta\mathrm{d}} + \dot{\varphi}_{\delta\mathrm{q}} \tag{8}$$

where u_d, u_q, i_d and i_q are the d-q axis stator voltages and currents, respectively; L_d and L_q are the d-q axis stator inductances, respectively; $\varphi_{\delta\mathrm{d}}$ and $\varphi_{\delta\mathrm{q}}$ are the d-q axis stator flux linkages, respectively; R is the stator resistance; φ_f is the rotor flux linkage.

From (2) to (7), the synchronous generator can be described by state space equations as follows:

$$\begin{cases} \dot{\boldsymbol{x}} = \boldsymbol{f}(x) + \boldsymbol{B}(x)\boldsymbol{U} \\ \boldsymbol{y} = [i_D \quad i_Q]^\mathrm{T} = \boldsymbol{h}(\boldsymbol{x}) \end{cases} \tag{9}$$

where $x = \begin{bmatrix} x_1 & x_2 & x_3 & x_4 \end{bmatrix}^\mathrm{T} = \begin{bmatrix} \varphi_{\delta\mathrm{d}} & \varphi_{\delta\mathrm{q}} & \bar{\theta} & \omega \end{bmatrix}^\mathrm{T}$, $\boldsymbol{h}(\boldsymbol{x}) = \begin{bmatrix} \frac{x_2}{L_\mathrm{q}}\cos\bar{\theta} - \frac{x_1-\varphi_\mathrm{f}}{L_\mathrm{d}}\sin\bar{\theta} \\ \frac{x_2}{L_\mathrm{q}}\sin\bar{\theta} - \frac{x_1-\varphi_\mathrm{f}}{L_\mathrm{d}}\cos\bar{\theta} \end{bmatrix}$,

$\boldsymbol{U} = \begin{bmatrix} u_\mathrm{D} & u_\mathrm{Q} \end{bmatrix}^\mathrm{T}$, $\boldsymbol{B}(x) = \begin{bmatrix} \cos\bar{\theta} & -\sin\bar{\theta} \\ \sin\bar{\theta} & \cos\bar{\theta} \\ 0 & 0 \\ 0 & 0 \end{bmatrix}$ and $\boldsymbol{f}(\boldsymbol{x}) = \begin{bmatrix} -\frac{R}{L_\mathrm{d}}x_1 + x_2x_4 - \frac{R}{L_\mathrm{d}}\varphi_\mathrm{f} \\ -\frac{R}{L_\mathrm{q}}x_2 - x_1x_4 \\ x_4 \\ 0 \end{bmatrix}$.

For the fully digital implementation, the system model (9) can be re-written in the following discrete form:

$$\begin{cases} \boldsymbol{x}_{k+1} = \boldsymbol{F}_d(x_k) + \boldsymbol{D}(x_k)\boldsymbol{u}_k + \boldsymbol{V}_k \\ \boldsymbol{y}_k = \boldsymbol{h}(\boldsymbol{x}_k) + \boldsymbol{W}_k \end{cases} \tag{10}$$

where $\boldsymbol{V}_k$ and $\boldsymbol{W}_k$ are the zero-mean Gaussian random vectors describing the model disturbances and the measurement disturbances with respective variance matrices of $\boldsymbol{Q}$ and $\boldsymbol{R}$; $\boldsymbol{F}_d(x_k) = \boldsymbol{x}_k + T_\mathrm{c}\boldsymbol{f}(\boldsymbol{x}(kT_\mathrm{c}))$; $\boldsymbol{D}(x_k) = T_\mathrm{c}B(\boldsymbol{x}(kT_\mathrm{c}))$ and T_c is the sampling period.

$\boldsymbol{x}_{k+1}$ can be estimated by EKF as follows:

Step 1: Prediction step

$$\begin{aligned} \tilde{\boldsymbol{x}}_{k+1} &= \boldsymbol{F}_d(x_k) + \boldsymbol{D}(x_k)\boldsymbol{u}_k \\ \tilde{\boldsymbol{y}}_{k+1} &= \boldsymbol{h}(\tilde{\boldsymbol{x}}_{k+1}) \\ \tilde{\boldsymbol{P}}_{k+1} &= \boldsymbol{F}_k\boldsymbol{P}_k\boldsymbol{F}_k^\mathrm{T} + \boldsymbol{Q}. \end{aligned}$$

Step 2: Innovation step

$$\begin{aligned} \boldsymbol{K}_{k+1} &= \tilde{\boldsymbol{P}}_{k+1}\boldsymbol{H}_{k+1}^\mathrm{T}\left[\boldsymbol{H}_{k+1}\tilde{\boldsymbol{P}}_{k+1}\boldsymbol{H}_{k+1}^\mathrm{T} + \boldsymbol{R}\right]^{-1} \\ \boldsymbol{x}_{k+1} &= \tilde{\boldsymbol{x}}_{k+1} + K_{k+1}\left[\boldsymbol{y}_{k+1} - \tilde{\boldsymbol{y}}_{k+1}\right] \\ \boldsymbol{P}_{k+1} &= \tilde{\boldsymbol{P}}_{k+1} - \boldsymbol{K}_{k+1}\boldsymbol{H}_{k+1}\tilde{\boldsymbol{P}}_{k+1} \end{aligned}$$

where $\boldsymbol{F}_k = \left.\frac{\partial \boldsymbol{f}(\boldsymbol{x})}{\partial \boldsymbol{x}}\right|_{\boldsymbol{x}=\boldsymbol{x}_k}$ and $\boldsymbol{H}_k = \left.\frac{\partial \boldsymbol{h}(\boldsymbol{x})}{\partial \boldsymbol{x}}\right|_{\boldsymbol{x}=\boldsymbol{x}_k}$ are the Jacobian matrices.

The values of $\varphi_{\delta\mathrm{d}}$ and $\varphi_{\delta\mathrm{q}}$ are obtained by EKF estimation

DOI: 10.1002/rnc

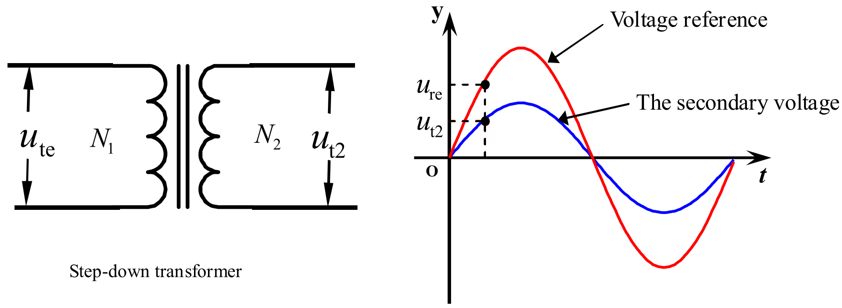

u_{te} - Instantaneous voltage of the generator terminal voltage; u_{t2} - Instantaneous secondary voltage of the step-down transformer;

u_{re} - Instantaneous voltage of the voltage reference; N_1- Turns of the primary windings;

N_2- Turns of the secondary windings

Figure 1. Voltage sampling by the AC tracking comparison.

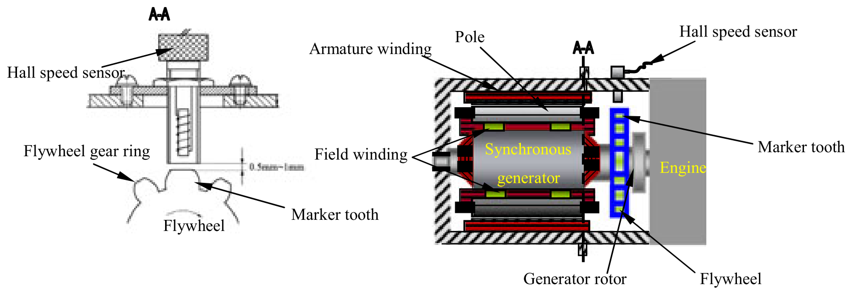

Figure 2. Local relation between the speed sensor and the flywheel.

3.2. Voltage sampling by AC tracking comparison

As shown in Figure 1, the voltage reference where the amplitude of which is invariable, has the same frequency and phase as the secondary voltage of the step-down transformer.

The RMS value of the generator terminal voltage u_{te} can be calculated by

$$U_{te} = K \frac{u_{t2}}{u_{re}} U_{re} \tag{11}$$

where U_{re} represents the RMS value of u_{re} and is constant, $K = \frac{N_1}{N_2}$ is the voltage ratio of the transformer and U_{te} is the RMS value of u_{te}.

U_{te} is usually obtained by the rectifier and filter circuit. The time constant of the filter circuit is large, thus affecting the excitation control speed. In this paper, from (11), U_{te} is obtained by the instantaneous values of the terminal voltage and the voltage reference. The sampling time constant is small, thus enabling voltage sampling by AC tracking comparison (VS-ACTC) to improve the excitation control speed.

In VS-ACTC, u_{re} must have the same frequency and phase as u_{t2}, which is realised as follows.

As shown in Figure 2, the electronic speed sensor is installed on MMPS. A wider tooth of the flywheel ring gear can be taken as the marker tooth. The flywheel was fixed and connected to the generator rotor, such that the positions of the marker tooth and φ_f are fixed. We suppose that φ_f lags the marker tooth by γ degree.

When the generator rotor rotates, we can obtain the voltage signal u_{speed} using the speed sensor, as shown in Figure 3. The phase diagram of the flux linkage and the voltage can be shown in Figure 4 based on (2) to (8).

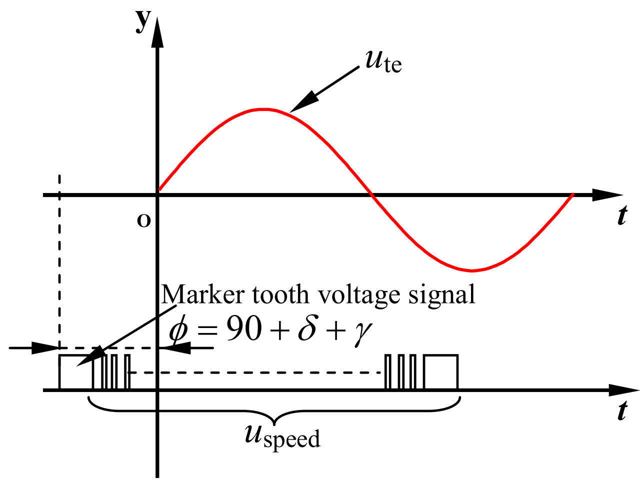

Figure 3. Phase relation between u_{te} and u_{speed}.

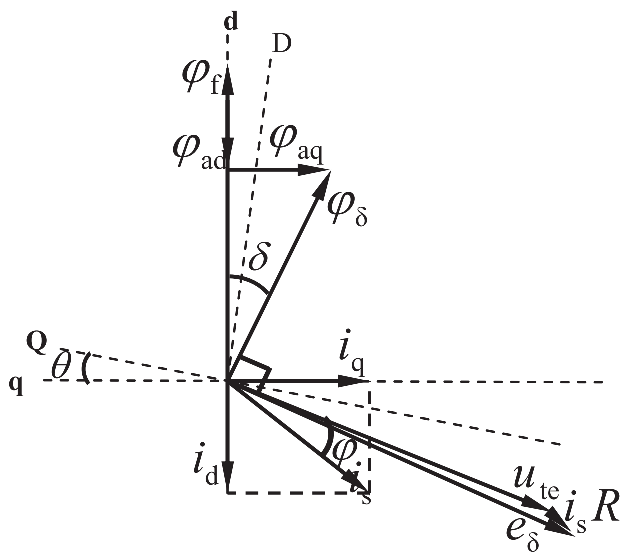

(D, Q) Stator frame; (d, q) Rotor frame

Figure 4. Phase diagram of voltage and flux linkage.

Figure 4 shows that u_{te} lags φ_δ by 90 degrees and φ_δ lags φ_f by δ degrees. u_{te} and u_{t2} have the same frequency and phase. Thus, u_{t2} lags the marker teeth by $90 + \delta + \gamma$ degrees.

Supposing that the numbers of the flywheel gear ring teeth and the generator pole-pairs are Z and P, we can obtain $\frac{Z}{P} = \text{n}$. The sinusoidal tabular data 0X0FFFH $\times \sin \frac{360}{k}(k = 1 \ldots n)$ can then be obtained and stored into the read only memory (ROM) of the CPU.

Figure 3 shows that if the CPU extracts the sinusoidal tabular data from the ROM lagging $90 + \gamma + \delta$ degrees at every rising edge of u_{speed} beginning with the voltage signal of the marker tooth and then controls the D/A output, the voltage reference u_{re} can be obtained. u_{re} will have the same phase and frequency as u_{te}. When the loads of the MMPS change, the value of the power angle δ also differs. In this paper, δ is calculated using $\delta = ar\tan\left(\frac{\varphi_{\delta d}}{\varphi_{\delta q}}\right)$. $\varphi_{\delta d}$, and $\varphi_{\delta q}$ are estimated by EKF, which is introduced in Section 3.1.

4. AC TRACKING OPTIMAL BACK-STEPPING ROBUST ADAPTIVE EXCITATION CONTROL

4.1. Optimal back-stepping robust adaptive control

We consider the following parametric strict-feedback system form:

$$\dot{x}_1 = f_1(x_1) + g_1(x_1)x_2 + \boldsymbol{\varphi}_1^{\mathrm{T}}(x_1)\boldsymbol{\theta} + \varepsilon_1 \tag{12.1}$$

$$\dot{x}_2 = f_2(x_1, x_2) + g_2(x_1, x_2)x_3 + \boldsymbol{\varphi}_2^{\mathrm{T}}(x_1, x_2)\boldsymbol{\theta} + \varepsilon_2 \tag{12.2}$$

$$\dot{x}_i = f_i(x_1, \ldots, x_i) + g_i(x_1, \ldots, x_i)x_{i+1} + \boldsymbol{\varphi}_i^{\mathrm{T}}(x_1, \ldots, x_i)\boldsymbol{\theta} + \varepsilon_i \tag{12.3}$$

$$\dot{x}_n = f_n(x_1, \ldots, x_n) + g_n(x_1, \ldots, x_n)u + \boldsymbol{\varphi}_n^{\mathrm{T}}(x_1, \ldots, x_n)\boldsymbol{\theta} + \varepsilon_n \tag{12.4}$$

where $\boldsymbol{x} \in \boldsymbol{R}^n$ is the state vector; $u \in \boldsymbol{R}$ is the control input; f_i, g_i and $i = 1, 2, \cdots n$ are smooth functions; $f_i(0) = 0$, $g_i(x_1, \ldots x_i) \neq 0$ and $\boldsymbol{\varphi}_i(x_1, \ldots x_i)$ are smooth vector fields; $\boldsymbol{\theta} \in R^p$ $(1 < p \leqslant n)$ is the unknown constant vector; ε_i $(i = 1, 2, \cdots n)$ is the unknown additive disturbance in L_2 space.

Step 1: Let $e_1 = x_1$, (12.1) can be used to obtain

$$\dot{e}_1 = f_1(x_1) + g_1(x_1)x_2 + \boldsymbol{\varphi}_1^{\mathrm{T}}(x_1)\boldsymbol{\theta} + \varepsilon_1. \tag{13}$$

Designing the stabilising function

$$x_2^* = \frac{1}{g_1(x_1)}\left[-f_1(x_1) - \boldsymbol{\varphi}_1^{\mathrm{T}}(x_1)\hat{\boldsymbol{\theta}} - m_1 e_1\right] \tag{14}$$

where $m_1 > 0$, $\hat{\boldsymbol{\theta}}$ is the estimated parameter vector of $\boldsymbol{\theta}$ and x_2^* is the virtual control.

When $\tilde{\boldsymbol{\theta}} = \boldsymbol{\theta} - \hat{\boldsymbol{\theta}}$ and $e_2 = x_2 - x_2^*$, substituting (14) into (13), we can use (12.2) to obtain

$$\dot{e}_1 = -m_1 e_1 + \boldsymbol{\varphi}_1^{\mathrm{T}}(x_1)\tilde{\boldsymbol{\theta}} + g_1(x_1)e_2 + \varepsilon_1 \tag{15}$$

$$\begin{aligned}\dot{e}_2 = \dot{x}_2 - \dot{x}_2^* &= f_2 + g_2 x_3 + \boldsymbol{\varphi}_2^{\mathrm{T}}\boldsymbol{\theta} - \frac{\partial x_2^*}{\partial x_1}\dot{x}_1 - \frac{\partial x_2^*}{\partial \hat{\boldsymbol{\theta}}}\dot{\hat{\boldsymbol{\theta}}} + \varepsilon_2 \\ &= f_2 + g_2 x_3 + \boldsymbol{\varphi}_2^{\mathrm{T}}\boldsymbol{\theta} - \frac{\partial x_2^*}{\partial x_1}\left(f_1 + g_1 x_2 + \boldsymbol{\varphi}_1^{\mathrm{T}}\boldsymbol{\theta} + \varepsilon_1\right) - \frac{\partial x_2^*}{\partial \hat{\boldsymbol{\theta}}}\dot{\hat{\boldsymbol{\theta}}} + \varepsilon_2.\end{aligned} \tag{16}$$

We then define

$$V_1 = \frac{e_1^2}{2} \tag{17}$$

$$V_2 = \frac{e_1^2}{2} + \frac{e_2^2}{2}. \tag{18}$$

Taking the derivative of (17) and (18) along with (15) and (16) yields

$$\dot{V}_1 = -m_1 e_1^2 + e_1\boldsymbol{\varphi}_1^{\mathrm{T}}(x_1)\tilde{\boldsymbol{\theta}} + e_1 g_1 e_2 + e_1\varepsilon_1 \tag{19}$$

DOI: 10.1002/rnc

$$\dot{V}_2 = -m_1 e_1^2 + e_1 \boldsymbol{\varphi}_1^{\mathrm{T}}(x_1)\tilde{\boldsymbol{\theta}} + e_2\left[g_1 e_1 + f_2 + g_2 x_3 + \boldsymbol{\varphi}_2^{\mathrm{T}}\boldsymbol{\theta} - \frac{\partial x_2^*}{\partial x_1}\left(f_1 + g_1 x_2 + \boldsymbol{\varphi}_1^{\mathrm{T}}\boldsymbol{\theta}\right) - \frac{\partial x_2^*}{\partial \hat{\boldsymbol{\theta}}}\dot{\hat{\boldsymbol{\theta}}}\right] + e_1\varepsilon_1 + e_2\varepsilon_2 - e_2\frac{\partial x_2^*}{\partial x_1}\varepsilon_1. \tag{20}$$

We design the virtual control x_3^* as

$$x_3^* = \frac{1}{g_2}\left[-g_1 e_1 - f_2 - \boldsymbol{\varphi}_2^{\mathrm{T}}\hat{\boldsymbol{\theta}} + \frac{\partial x_2^*}{\partial x_1}\left(f_1 + g_1 x_2 + \boldsymbol{\varphi}_1^{\mathrm{T}}\hat{\boldsymbol{\theta}}\right) + \frac{\partial x_2^*}{\partial \hat{\boldsymbol{\theta}}}\dot{\hat{\boldsymbol{\theta}}} - m_2 e_2\right] \tag{21}$$

where $m_2 > 0$.

When $e_3 = x_3 - x_3^*$, substituting (21) into (16) and (20), we obtain

$$\dot{e}_2 = -m_2 e_2 + \boldsymbol{\varphi}_2^{\mathrm{T}}\tilde{\boldsymbol{\theta}} + g_2 e_3 - g_1 e_1 - \frac{\partial x_2^*}{\partial x_1}\boldsymbol{\varphi}_1^{\mathrm{T}}\tilde{\boldsymbol{\theta}} + \varepsilon_2 - \frac{\partial x_2^*}{\partial x_1}\varepsilon_1 \tag{22}$$

$$\dot{V}_2 = -\sum_{j=1}^{2} m_j e_j^2 + \sum_{j=1}^{2} e_j \boldsymbol{\varphi}_j^{\mathrm{T}}\tilde{\boldsymbol{\theta}} + \sum_{j=1}^{2} e_j\varepsilon_j - e_2\frac{\partial x_2^*}{\partial x_1}\boldsymbol{\varphi}_1^{T}\tilde{\boldsymbol{\theta}} + g_2 e_2 e_3 - e_2\frac{\partial x_2^*}{\partial x_1}\varepsilon_1. \tag{23}$$

Step i:

$$V_i = \sum_{j=1}^{i} \frac{e_j^2}{2} \tag{24}$$

$$\dot{V}_i = -\sum_{j=1}^{i} m_j e_j^2 + \sum_{j=1}^{i} e_j \boldsymbol{\varphi}_j^{\mathrm{T}}\tilde{\boldsymbol{\theta}} + \sum_{j=1}^{i} e_j\varepsilon_j - \sum_{k=2}^{i}\sum_{j=1}^{k-1} e_k \frac{\partial x_k^*}{\partial x_j}\boldsymbol{\varphi}_j^{\mathrm{T}}\tilde{\boldsymbol{\theta}} + g_i e_i e_{i+1} + \sum_{k=2}^{i}\sum_{j=1}^{k-1} e_k \frac{\partial x_k^*}{\partial x_j}\varepsilon_j \tag{25}$$

$$\dot{e}_i = -m_i e_i + \boldsymbol{\varphi}_i^{\mathrm{T}}\tilde{\boldsymbol{\theta}} + g_i e_{i+1} - g_{i-1}e_{i-1} - \sum_{j=1}^{i-1}\frac{\partial x_i^*}{\partial x_j}\boldsymbol{\varphi}_j^{\mathrm{T}}\tilde{\boldsymbol{\theta}} + \varepsilon_i - \sum_{j=1}^{i-1}\frac{\partial x_i^*}{\partial x_j}\varepsilon_j. \tag{26}$$

Step n: We define

$$V_n = V_{n-1} + \frac{1}{2}e_n^2 + \frac{1}{2}\tilde{\boldsymbol{\theta}}^{\mathrm{T}}\boldsymbol{\Gamma}^{-1}\tilde{\boldsymbol{\theta}}. \tag{27}$$

Taking the derivative of (27) yields

$$\dot{V}_n = \dot{V}_{n-1} + e_n\dot{e}_n + \tilde{\boldsymbol{\theta}}^{\mathrm{T}}\boldsymbol{\Gamma}^{-1}\dot{\tilde{\boldsymbol{\theta}}}. \tag{28}$$

Using (25) and (26), we can obtain

$$\dot{V}_n = -\sum_{j=1}^{n-1} m_j e_j^2 + \sum_{j=1}^{n-1} e_j\varepsilon_j + \sum_{j=1}^{n-1} e_j\boldsymbol{\varphi}_j^{\mathrm{T}}\tilde{\boldsymbol{\theta}} - \sum_{k=2}^{n-1}\sum_{j=1}^{k-1} e_k\frac{\partial x_{\mathrm{k}}^*}{\partial x_j}\boldsymbol{\varphi}_j^{\mathrm{T}}\tilde{\boldsymbol{\theta}} - \tilde{\boldsymbol{\theta}}^{\mathrm{T}}\boldsymbol{\Gamma}^{-1}\dot{\hat{\boldsymbol{\theta}}} - \sum_{k=2}^{n-1}\sum_{j=1}^{k-1} e_k\frac{\partial x_{\mathrm{k}}^*}{\partial x_j}\varepsilon_j + e_n\left[g_{n-1}e_{n-1} + f_n + g_n u + \boldsymbol{\varphi}_n^{\mathrm{T}}\boldsymbol{\theta} + \varepsilon_n - \sum_{j=1}^{n-1}\frac{\partial x_n^*}{\partial x_j}\left(f_j + g_j x_{j+1} + \boldsymbol{\varphi}_j^{\mathrm{T}}\boldsymbol{\theta} + \varepsilon_j\right) - \frac{\partial x_n^*}{\partial \hat{\boldsymbol{\theta}}}\dot{\hat{\boldsymbol{\theta}}}\right]. \tag{29}$$

The control input u and the adaptive law of $\hat{\boldsymbol{\theta}}$ can be respectively designed as

$$u = \frac{1}{g_n}\left[-g_{n-1}e_{n-1} - f_n - \boldsymbol{\varphi}_n^T\hat{\boldsymbol{\theta}} + \sum_{j=1}^{n-1}\frac{\partial x_n^*}{\partial x_j}\left(f_j + g_j x_{j+1} + \boldsymbol{\varphi}_j^{\mathrm{T}}\hat{\boldsymbol{\theta}}\right) + \frac{\partial x_n^*}{\partial \hat{\boldsymbol{\theta}}}\dot{\hat{\boldsymbol{\theta}}} - m_n e_n - u_{\mathrm{f1}}\right] \tag{30}$$

$$\dot{\hat{\boldsymbol{\theta}}} = \left[\left(\sum_{j=1}^{n-1} e_j\boldsymbol{\varphi}_j^{\mathrm{T}} - \sum_{k=2}^{n}\sum_{j=1}^{k-1} e_k\frac{\partial x_{\mathrm{k}}^*}{\partial x_j}\boldsymbol{\varphi}_j^{\mathrm{T}}\right)\boldsymbol{\Gamma}\right]^{\mathrm{T}} \tag{31}$$

where $m_{\mathrm{n}} > 0$ and u_{f1} is the additive control.

When substituting (30) and (31) into (29), we obtain

$$\dot{V}_n = -\sum_{j=1}^{n} m_j e_j^2 + \sum_{j=1}^{n} e_j\varepsilon_j - \sum_{k=2}^{n-1}\sum_{j=1}^{k-1} e_k\frac{\partial x_{\mathrm{k}}^*}{\partial x_j}\varepsilon_j - e_n u_{\mathrm{f1}}. \tag{32}$$

Remark 1

The following closed-loop error system can be obtained using the back-stepping method:

$$\dot{e}_1 = -m_1 e_1 + \boldsymbol{\varphi}_1^{\mathrm{T}}\tilde{\boldsymbol{\theta}} + g_1 e_2 + \varepsilon_1 \tag{33.1}$$

$$\dot{e}_i = -m_i e_i + \boldsymbol{\varphi}_i^{\mathrm{T}}\tilde{\boldsymbol{\theta}} + g_i e_{i+1} - g_{i\text{-}1}e_{i\text{-}1} - \sum_{j=1}^{i-1}\frac{\partial x_i^*}{\partial x_j}\boldsymbol{\varphi}_j^{\mathrm{T}}\tilde{\boldsymbol{\theta}} + \varepsilon_i - \sum_{j=1}^{i-1}\frac{\partial x_i^*}{\partial x_j}\varepsilon_j \tag{33.2}$$

$$\dot{e}_n = -m_n e_n + u_{\mathrm{f1}} + \boldsymbol{\varphi}_n^{\mathrm{T}}\tilde{\boldsymbol{\theta}} - g_{n\text{-}1}e_{n\text{-}1} - \sum_{j=1}^{n-1}\frac{\partial x_{\mathrm{n}}^*}{\partial x_j}\boldsymbol{\varphi}_j^{\mathrm{T}}\tilde{\boldsymbol{\theta}} + \varepsilon_n - \sum_{j=1}^{n-1}\frac{\partial x_{\mathrm{n}}^*}{\partial x_j}\varepsilon_j \tag{33.3}$$

$$\dot{\hat{\boldsymbol{\theta}}} = \left[\left(\sum_{j=1}^{n-1} e_j\boldsymbol{\varphi}_j^{\mathrm{T}} - \sum_{k=2}^{n}\sum_{j=1}^{k-1} e_k\frac{\partial x_{\mathrm{k}}^*}{\partial x_j}\boldsymbol{\varphi}_j^{\mathrm{T}}\right)\boldsymbol{\Gamma}\right]^{\mathrm{T}}. \tag{33.4}$$

The design of the OBRAC can be discussed in following two kinds of circumstances:

(a) $\varepsilon_i = 0, i = 1, 2, \cdots n$

When $\varepsilon_i = 0$, we can obtain $\dot{V}_n = -\sum_{j=1}^{n} m_j e_j^2 - u_{\mathrm{f1}}e_n$ using (32).

When $u_{\mathrm{f1}} = Ke_n$ $(K > 0)$, then $\dot{V}_n = -\sum_{j=1}^{n} m_j e_j^2 - Ke_n^2 \leqslant 0$. Substituting $u_{\mathrm{f1}} = Ke_n$ into (30), we obtain the control input u.

Remark 2

When $m_j > 0 (j = 1, 2, \cdots n)$ and $K > 0$, $V_n = V_{n-1} + \frac{1}{2}e_n^2 + \frac{1}{2}\tilde{\boldsymbol{\theta}}^{\mathrm{T}}\boldsymbol{\Gamma}^{-1}\tilde{\boldsymbol{\theta}} \geqslant 0$ and $\dot{V}_n \leqslant 0$. The controller is adaptive to uncertain parameter $\boldsymbol{\theta}$ and can stabilise the system, but cannot realise the optimal control. m_j and K, standing for any positive constants, are the lack of the optimal restraint. The adaptive law is expressed by (33.4).

DOI: 10.1002/rnc

When $\varepsilon_i = 0$ and direct feedback linearization (DFL) is used in (33), we obtain

$$\dot{z}_1 = z_2 = \dot{e}_1 = -m_1 e_1 + \boldsymbol{\varphi}_1^{\mathrm{T}} \tilde{\boldsymbol{\theta}} + g_1 e_2 \tag{34.1}$$

$$\dot{z}_2 = z_3 = -m_1 \dot{e}_1 + \dot{\boldsymbol{\varphi}}_1^{\mathrm{T}} \tilde{\boldsymbol{\theta}} + \boldsymbol{\varphi}_1^{\mathrm{T}} \dot{\tilde{\boldsymbol{\theta}}} + \dot{g}_1 e_2 + g_1 \dot{e}_2 \tag{34.2}$$

$$\dot{z}_n = f(z_1, \ldots, z_n) + bv \tag{34.3}$$

or

$$\dot{\boldsymbol{Z}} = \boldsymbol{A}\boldsymbol{Z} + \boldsymbol{B}v \tag{35}$$

where $f(z_1, \ldots z_{\mathrm{n}})$ is the linear function, $\boldsymbol{A}$ is a constant matrix, $\boldsymbol{B} = [0\ 0 \cdots 0\ 1]^{\mathrm{T}}$ and $v = f(u_{\mathrm{f1}})$.

For the linear system (35), the quadratic performance index can be expressed as

$$\boldsymbol{J} = \frac{1}{2} \int_0^{\infty} \left(\boldsymbol{Z}^{\mathrm{T}} \boldsymbol{Q} \boldsymbol{Z} + v^{\mathrm{T}} \boldsymbol{R} v \right) dt \tag{36}$$

where $\boldsymbol{Q}$ is the semi-positive weighting matrix and $\boldsymbol{R}$ is the positive weighting matrix.

Based on the linear quadratic regulation principle, the optimal control input is $v = \boldsymbol{R}^{-1}\boldsymbol{B}^{\mathrm{T}}\boldsymbol{P}\boldsymbol{Z}$, where $\boldsymbol{P}$ is the solution of the Riccati equation $\boldsymbol{A}^{\mathrm{T}}\boldsymbol{P} + \boldsymbol{P}\boldsymbol{A} - \boldsymbol{P}\boldsymbol{B}\boldsymbol{R}^{-1}\boldsymbol{B}^{T}\boldsymbol{P} + \boldsymbol{Q} = 0$.

Substituting $v = \boldsymbol{R}^{-1}\boldsymbol{B}^{\mathrm{T}}\boldsymbol{P}\boldsymbol{Z}$ into $u_{\mathrm{f1}} = f^{-1}(v)$ and (30), we obtain the value of u (the OBRAC input).

Remark 3

If an optimal solution of the linear system (35) exists, the system should be stable, and $\dot{V}_n \leqslant 0$ and $e_i \to 0$, $i = 1, 2, \cdots n$. The control input u can stabilise the system and realise the optimal control of the uncertain system. The adaptive law is expressed by (33.4).

(b) $\varepsilon_i \neq 0, i = 1, 2, \cdots n$

When $\varepsilon_i \neq 0$ and DFL is used in (33), we obtain

$$\dot{e}_1 = \dot{z}_1 = z_2 + \varepsilon_1 = -m_1 e_1 + \boldsymbol{\varphi}_1^{\mathrm{T}} \tilde{\boldsymbol{\theta}} + g_1 e_2 + \varepsilon_1 \tag{37.1}$$

$$\begin{aligned}\dot{z}_2 &= -m_1 \dot{e}_1 + \dot{\boldsymbol{\varphi}}_1^{\mathrm{T}} \tilde{\boldsymbol{\theta}} + \boldsymbol{\varphi}_1^{\mathrm{T}} \dot{\tilde{\boldsymbol{\theta}}} + \dot{g}_1 e_2 + g_1 \dot{e}_2 = -m_1 z_1 + \dot{\boldsymbol{\varphi}}_1^{\mathrm{T}} \tilde{\boldsymbol{\theta}} + \boldsymbol{\varphi}_1^{\mathrm{T}} \dot{\tilde{\boldsymbol{\theta}}} + \dot{g}_1 e_2 \\ &\quad + g_1 \left(-m_2 e_2 + \boldsymbol{\varphi}_2^{\mathrm{T}} \tilde{\boldsymbol{\theta}} - g_1 e_1 - \frac{\partial x_2^*}{\partial x_1} \boldsymbol{\varphi}_1^{\mathrm{T}} \tilde{\boldsymbol{\theta}} + g_2 e_3 + \varepsilon_2 - \frac{\partial x_2^*}{\partial x_1} \varepsilon_1 \right) \\ &= z_3 + \varepsilon_2 - \frac{\partial x_2^*}{\partial x_1} \varepsilon_1\end{aligned} \tag{37.2}$$

$$\dot{z}_n = f(z_1, \ldots, z_n) + f(\varepsilon_1, \ldots, \varepsilon_n) + bv. \tag{37.3}$$

Or

$$\dot{\boldsymbol{Z}} = \boldsymbol{A}\boldsymbol{Z} + \boldsymbol{B}_1 \boldsymbol{w} + \boldsymbol{B}_2 v \tag{38}$$

where $\boldsymbol{A}$ is the constant matrix, $\boldsymbol{B}_1 = \boldsymbol{I}$, $w = [w_1\ w_2\ \cdots w_n]^{\mathrm{T}}$, $w_1 = \varepsilon_1$, $w_2 = \varepsilon_2 - \frac{\partial x_2^*}{\partial x_1}\varepsilon_1, \ldots, w_n = \varepsilon_n - \sum_{j=1}^{n-1} \frac{\partial x_{\mathrm{n}}^*}{\partial x_j}\varepsilon_j$, $\boldsymbol{B}_2 = [0\ 0 \cdots 0\ 1]^{\mathrm{T}}$ and $v = f(u_{\mathrm{f1}})$.

When $\boldsymbol{y} = \boldsymbol{C}\boldsymbol{Z}$, considering that $\gamma > 0$ and if the system satisfies $\int_0^T (\|y\|^2 + \|v\|^2) dt \leqslant \gamma^2 \int_0^T (\|\varepsilon\|^2) dt$, we can confirm that system (38) has an L2 gain less than or equal to γ, and the optimal control law and the worst disturbance are as follows:

$$v = \boldsymbol{W}\boldsymbol{P}^{-1} \tag{39}$$

$$\boldsymbol{w} = -\frac{1}{\gamma^2}\boldsymbol{B}_1^{\mathrm{T}}\boldsymbol{P}\boldsymbol{Z} \tag{40}$$

where $\boldsymbol{W}$ and $\boldsymbol{P}$ are the solutions of the following LMI (41):

$$\begin{bmatrix} \boldsymbol{A}\boldsymbol{P} + \boldsymbol{B}_2\boldsymbol{W} + (\boldsymbol{A}\boldsymbol{P} + \boldsymbol{B}_2\boldsymbol{W})^{\mathrm{T}} & \boldsymbol{B}_1 & \boldsymbol{P}\boldsymbol{C}^{\mathrm{T}} \\ \boldsymbol{B}_1^{\mathrm{T}} & -\boldsymbol{I} & 0 \\ \boldsymbol{C}\boldsymbol{P} & 0 & -\gamma^2\boldsymbol{I} \end{bmatrix} < 0. \tag{41}$$

Substituting (39) into $u_{\mathrm{f1}} = f^{-1}(v)$ and (30), we can obtain u (the optimal back-stepping robust adaptive L2 gain attenuation control input). The adaptive law is expressed by (33.4).

Remark 4

For the parametric strict-feedback nonlinear system with uncertain parameters and disturbances, the OBRAC controller is adaptive to uncertain parameters and robust to w_i (unknown additive disturbance). Moreover, the OBRAC controller can be applied to minimise the effect of disturbance by solving the LMI to obtain the optimal control law against the worst disturbance.

4.2. *Optimal back-stepping robust adaptive excitation control*

For the excitation system (1), the deduction of OBRAEC can be described as follows:

Step 1: Let $e_1 = x_1$, $x_2^* = -m_1e_1$ and $e_2 = x_2 - x_2^*$, we use (1.1) and (1.2) to obtain

$$\dot{e}_1 = \dot{x}_1 = x_2 = -m_1e_1 + e_2 \tag{42}$$

$$\dot{e}_2 = \dot{x}_2 - \dot{x}_2^* = -\theta - \beta_1\sin(\delta_0 + x_1)x_3 - \beta_1x_{30}[\sin(\delta_0 + x_1) - \sin(\delta_0)] + \varepsilon_2 + m_1x_2 \tag{43}$$

where $m_1 > 0$, θ is the unknown parameter and $\hat{\theta}$ is the estimate of θ.

Step 2: We define $V_1 = \frac{e_1^2}{2}$ and $V_2 = \frac{e_1^2}{2} + \frac{e_2^2}{2}$. We take the derivative of V_1, V_2 along (42), (43) to obtain

$$\begin{aligned}\dot{V}_2 = e_1\dot{e}_1 + e_2\dot{e}_2 = -m_1e_1^2 + e_2\{e_1 - \beta_1\sin(\delta_0 + x_1)x_3 + m_1x_2 - \beta_1x_{30} \\ \times[\sin(\delta_0 + x_1) - \sin(\delta_0)] - \theta\} + e_2\varepsilon_1.\end{aligned} \tag{44}$$

We design the stabilising function x_3^* as follows:

$$x_3^* = \frac{1}{\beta_1\sin(\delta_0 + x_1)}\left\{e_1 - \hat{\theta} + m_1x_2 - m_2e_2 - \beta_1x_{30}[\sin(\delta_0 + x_1) - \sin(\delta_0)]\right\} \tag{45}$$

where $m_2 > 0$.

When $e_3 = x_3 - x_3^*$, substituting (45) into (43), we obtain

$$\dot{e}_2 = \dot{x}_2 - \dot{x}_2^* = -m_2e_2 - e_1 - \tilde{\theta} - \beta_1\sin(\delta_0 + x_1)e_3 + \varepsilon_1. \tag{46}$$

Step 3: Let $V_3 = V_2 + \frac{e_3^2}{2} + \frac{1}{2\rho}\tilde{\theta}^2$, $e_3 = x_3 - x_3^*$, the derivative of V_3 is taken along (42) and (46). Using (1.3), we obtain

$$\begin{aligned}\dot{V}_3 = &-\sum_{j=1}^{2} m_je_j^2 + \tilde{\theta}e_2 - \frac{1}{\rho}\tilde{\theta}\dot{\hat{\theta}} + \frac{(m_1 + m_2)x_2}{\beta_1\sin(\delta_0 + x_1)}e_3\tilde{\theta} + e_2\varepsilon_1 \\ &+ e_3\left\{-\beta_1\sin(\delta_0 + x_1)e_2 - \beta_2x_3 - \beta_3[\cos(\delta_0) - \cos(\delta_0 + x_1)] + \frac{u}{T_{\mathrm{d0}}} + \varepsilon_2 - \dot{x}_3^*\right\}.\end{aligned} \tag{47}$$

DOI: 10.1002/rnc

The control input and the adaptive law are designed as (48) and (49), respectively.

$$u=T_{\mathrm{d}0}\left\{\begin{array}{l}\beta_1\sin(\delta_0+x_1)e_2+\beta_2x_3+\beta_3[\cos(\delta_0)-\cos(\delta_0+x_1)]-m_3e_3+u_{\mathrm{f}1}-\\ \dfrac{1}{\beta_1\sin(\delta_0+x_1)}\left\{\begin{array}{l}x_2-\beta_1x_{30}\cos(\delta_0+x_1)x_2+m_1m_2x_2-\\ \dot{\hat{\theta}}+(m_1+m_2)\left\{\begin{array}{l}-\hat{\theta}-\beta_1\sin(\delta_0+x_1)x_3-\\ \beta_1x_{30}[\sin(\delta_0+x_1)-\sin(\delta_0)]\end{array}\right\}\end{array}\right\}+\\ \dfrac{x_2\cos(\delta_0+x_1)\left\{-\hat{\theta}+e_1-\beta_1x_{30}[\sin(\delta_0+x_1)-\sin(\delta_0)]+m_1x_2+m_2e_2\right\}}{\beta_1\sin^2(\delta_0+x_1)}\end{array}\right\} \tag{48}$$

$$\dot{\hat{\theta}}=\rho\left[-e_2+\frac{(m_1+m_2)}{\beta_1u_{\mathrm{s}}\sin(\delta_0+x_1)}\right]. \tag{49}$$

Substituting (48) and (49) into (47) yields

$$\dot{V}_3=-\sum_{j=1}^{3}m_je_j^2+u_{\mathrm{f}1}e_3+e_2\varepsilon_1+e_3\varepsilon_2+\frac{e_3(m_1+m_2)}{\beta_1\sin(\delta_0+x_1)}\varepsilon_1. \tag{50}$$

By the back-stepping method, we obtain the following closed-loop error system:

$$\dot{e}_1=\dot{x}_1=x_2=-m_1e_1+e_2 \tag{50.1}$$

$$\dot{e}_2=-m_2e_2-e_1-\tilde{\theta}-\beta_1\sin(\delta_0+x_1)e_3+\varepsilon_1 \tag{50.2}$$

$$\dot{e}_3=\beta_1\sin(\delta_0+x_1)e_2-m_3e_3+u_{\mathrm{f}1}+\frac{(m_1+m_2)}{\beta_1\sin(\delta_0+x_1)}\tilde{\theta}+\varepsilon_2+\frac{(m_1+m_2)}{\beta_1\sin(\delta_0+x_1)}\varepsilon_1. \tag{50.3}$$

When DFL is used in (50), we obtain

$$\dot{z}_1=z_2=\dot{e}_1=-m_1e_1+e_2 \tag{51.1}$$

$$\dot{z}_2=-m_1\dot{e}_1+\dot{e}_2=\left(m_1^2-1\right)e_1-(m_1+m_2)\,e_2-\beta_1\sin(\delta_0+x_1)e_3-\tilde{\theta}+\varepsilon_1=z_3+\varepsilon_1 \tag{51.2}$$

$$\begin{aligned}\dot{z}_3&=-\dot{\hat{\theta}}+\left(m_1^2-1\right)\dot{e}_1-(m_1+m_2)\dot{e}_2-\beta_1\cos(\delta_0+x_1)x_2-\beta_1\sin(\delta_0+x_1)\dot{e}_3\\ &=\left(m_1^2-1\right)z_2+v_1-\frac{2m_1+2m_2}{\beta_1\sin(\delta_0+x_1)}\varepsilon_1-\varepsilon_2\\ &=-m_1\left(m_1^2-1\right)z_1+v_2-\frac{2m_1+2m_2}{\beta_1\sin(\delta_0+x_1)}\varepsilon_1-\varepsilon_2.\end{aligned} \tag{51.3}$$

(a) $\varepsilon_i=0, i=1,2,\cdots n$

From (51), we can obtain the state equation

$$\dot{\boldsymbol{Z}}\begin{bmatrix}\dot{z}_1\\ \dot{z}_2\\ \dot{z}_3\end{bmatrix}=\begin{bmatrix}0&1&0\\0&0&1\\0&m_1^2-1&0\end{bmatrix}\begin{bmatrix}z_1\\z_2\\z_3\end{bmatrix}+\begin{bmatrix}0\\0\\1\end{bmatrix}v_1=\boldsymbol{AZ}+\boldsymbol{B}v_1 \tag{52}$$

where

$$\begin{aligned}u_{\mathrm{f}1}=&\frac{-v_1+(m_1+m_2)(m_2e_2+e_1)}{\beta_1\sin(\delta_0+x_1)}+\dot{\hat{\theta}}\\ &+(m_1+m_2)e_3-\beta_1\sin(\delta_0+x_1)e_2+m_3e_3-\mathrm{ctan}(\delta_0+x_1)x_2e_3.\end{aligned} \tag{53}$$

Using optimisation control, the quadratic performance index is $\boldsymbol{J}=\frac{1}{2}\int_0^\infty\left(\boldsymbol{Z}^{\mathrm{T}}\boldsymbol{QZ}+v_1^{\mathrm{T}}\boldsymbol{R}v_1\right)dt$, and the optimal control input is $v_1=\boldsymbol{R}^{-1}\boldsymbol{B}^{\mathrm{T}}\boldsymbol{PZ}$. Substituting v_1

into (53), we can obtain u_{f1}. Substituting u_{f1} into (48), we obtain the control input u. The adaptive law is expressed by (49).

From (51), we can obtain $z_1 = e_1 = x_1 = \delta - \delta_0$, $z_2 = -m_1 e_1 + e_2 = x_2 = \omega - \omega_0$ and $z_3 = -m_1 \dot{e}_1 + \dot{e}_2 = \dot{x}_2 = \dot{\omega}$.

Remark 5

The OBRAEC controller is adaptive to uncertain parameters and can improve the convergence speed of $\delta - \delta_0$, $\omega - \omega_0$ and $\dot{\omega}$ by modifying the values of $\boldsymbol{Q}$ and $\boldsymbol{R}$. In OBRAEC, $\boldsymbol{J} = \frac{1}{2}\int_0^\infty \left(q_1(\delta - \delta_0)^2 + q_2(\omega - \omega_0)^2 + q_3\dot{\omega}^2 + v^2\right) dt = \boldsymbol{J}_{\min}$ will be realised.

(b) $\varepsilon_i \neq 0, i = 1, 2, \cdots n$

From (51), we obtain the following state equation:

$$\begin{bmatrix} \dot{z}_1 \\ \dot{z}_2 \\ \dot{z}_3 \end{bmatrix} = \begin{bmatrix} 0 & 1 & 0 \\ 0 & 0 & 1 \\ -m_1\left(m_1^2 - 1\right) & 0 & 0 \end{bmatrix} \begin{bmatrix} z_1 \\ z_2 \\ z_3 \end{bmatrix} + \begin{bmatrix} 0 & 0 \\ 1 & 0 \\ 0 & -1 \end{bmatrix} \begin{bmatrix} w_1 \\ w_2 \end{bmatrix} + \begin{bmatrix} 0 \\ 0 \\ 1 \end{bmatrix} v_2 \text{ or } \dot{\boldsymbol{Z}} = \boldsymbol{A}\boldsymbol{Z} + \boldsymbol{B}_1 w + \boldsymbol{B}_2 v_2 \tag{54}$$

where $w_1 = \varepsilon_1$, $w_2 = \hat{\theta}\varepsilon_1 + \beta_1 \sin(\delta_0 + x_1)\varepsilon_2$ and

$$u_{f1} = \frac{-v_2 + \left(m_1^2 - 1\right)e_2 + (m_1 + m_2)m_2 e_2}{\beta_1 \sin(\delta_0 + x_1)} + (m_1 + m_2)e_3 - \beta_1 \sin(\delta_0 + x_1)e_2 + m_3 e_3 + \dot{\hat{\theta}} - \beta_1 \cos(\delta_0 + x_1)x_1 e_3. \tag{55}$$

When $y = CZ$ and system (54) has an L2 gain less than or equal to γ, the optimal control law and the worst disturbance can be calculated by (39), (40) and (41).

Remark 6

When disturbances and uncertain parameters are present in the nonlinear excitation system, the OBRAEC controller is adaptive to the uncertain parameters and can realise L2 gain disturbance attenuation and the optimal control.

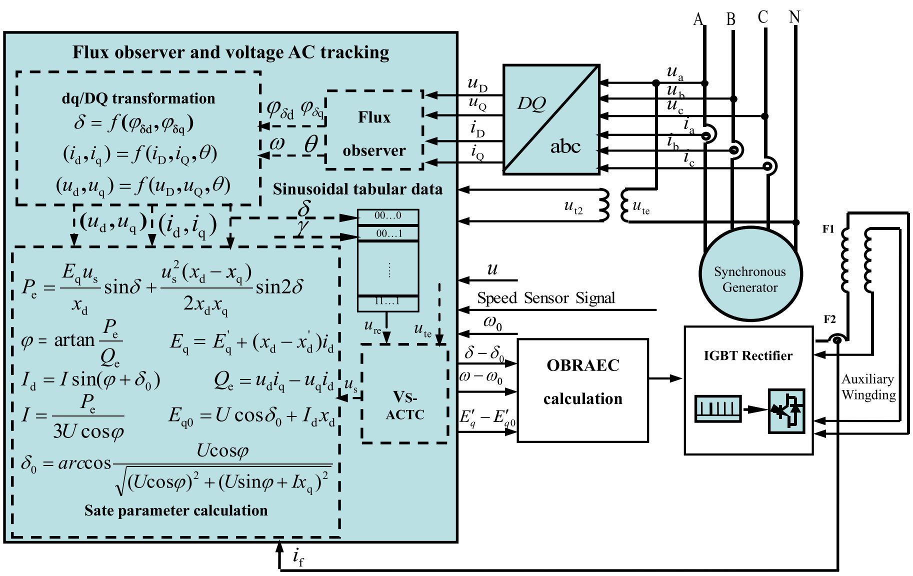

Figure 5. Block diagram of the AC tracking optimal back-stepping robust adaptive excitation control based on the state variable extended Kalman filter estimation.

4.3. *AC tracking OBRAEC based on the state tracing estimation by EKF*

The block diagram of the AC tracking OBRAEC is shown in Figure 5.

Using the flux linkage observer, the values of $\varphi_{\delta\text{d}}$, $\varphi_{\delta\text{q}}$ and $\bar{\theta}$ can be EKF estimated (introduced in Section 3.1). u_{D}, u_{Q}, i_{D} and i_{Q} are the inputs of the flux linkage observer and can be calculated by the transformation of stator voltage and stator current (introduced in Section 2). u_{d}, u_{q}, i_{d} and i_{q} can be calculated by the DQ/dq transformation of u_{D}, u_{Q}, i_{D} and i_{Q}, respectively (introduced in Section 2). The terminal voltage u_{s} can be obtained using VS-ACTC (introduced in Section 3.2). The state vector $[x_1\ x_2\ x_3]^{\text{T}} = \left[\delta - \delta_0\ \omega - \omega_0\ E'_q - E'_{q0}\right]^{\text{T}}$ on all operating points can be obtained with the estimates and calculations of $\varphi_{\delta\text{d}}$, $\varphi_{\delta\text{q}}$, u_{d}, u_{q}, i_{d} and i_{q} (introduced in Section 2). The OBRAEC can be realised using the value of the state vector (introduced in Section 4.2).

5. SIMULATION AND EXPERIMENT

Simulations and experiments were performed using the following parameters: $x_{\text{d}} = 1.25\,\text{p.u.}$, $x'_{\text{d}} = 0.221\,\text{p.u.}$, $M = 2.05\,s$, $T'_{\text{d}} = 1.05\,s$, $\delta_0 = 25.2°$, $\omega_0 = 1\,\text{p.u.}$, $E'_{\text{q}0} = 1.0\,\text{p.u.}$ and $D = 1\,\text{p.u.} - 5\,\text{p.u.}$ In the PID control, $D = 3\,\text{p.u.}$

5.1. *Flux linkage observation by extended Kalman filter*

When the load of the MMPS is suddenly increased at 0.53 s, the actual and EKF estimated values of $\varphi_{\delta\text{d}}$ and $\varphi_{\delta\text{q}}$ are shown in Figure 6(a) and (b), respectively.

The errors between the actual and estimated values of φ_δ are shown in Figure 7.

Figures 6 and 7 show that the error between the actual and estimated values is small. Thus, the location and the value of the flux linkage φ_δ can be correctly estimated by EKF.

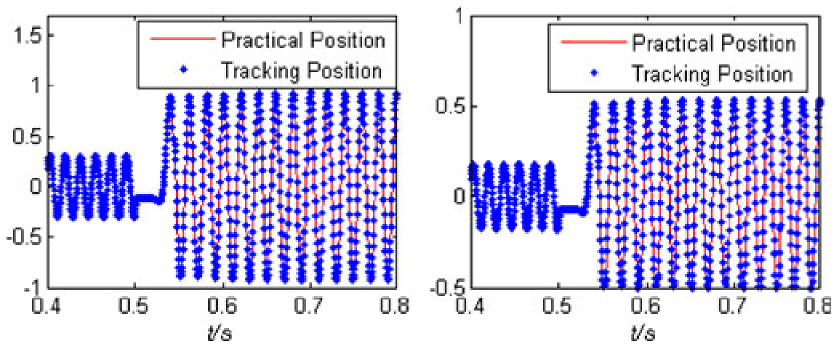

(a) $\varphi_{\delta\text{d}}$ (b) $\varphi_{\delta\text{q}}$

Figure 6. Comparison between the actual value and the estimated value.

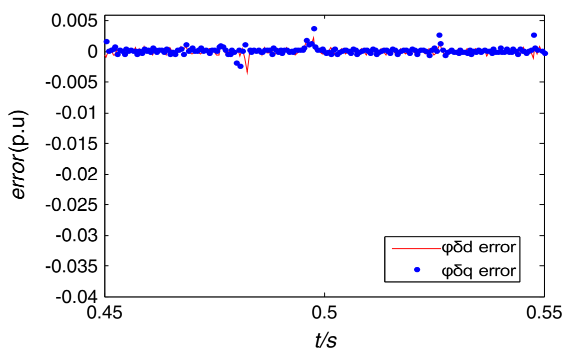

Figure 7. Error between the actual and estimated values of φ_δ.

DOI: 10.1002/rnc

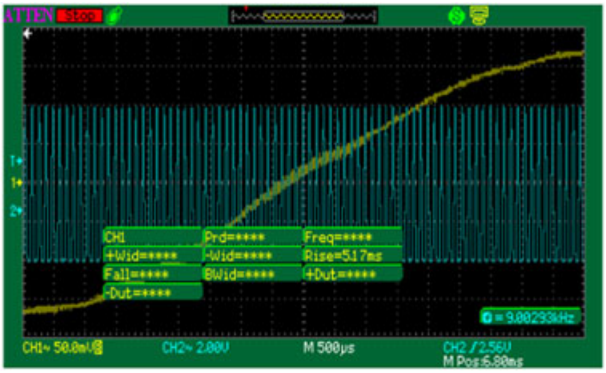

Figure 8. Speed sensor signal and the terminal voltage.

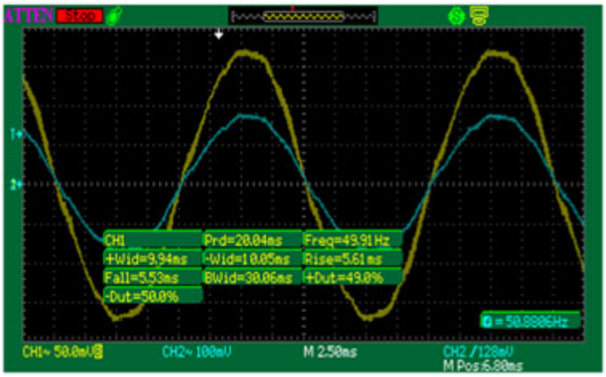

Figure 9. Voltage reference and the terminal voltage.

5.2. Measurement of the AC tracking voltage reference

To determine whether the voltage reference and the terminal voltage have the same frequency and phase, we test the waveforms of the generator terminal voltage and the voltage reference shown in Figures 8 and 9. The voltage reference is outputted from the D/A pin of the STM32F103ZET.

Figure 8 shows that the frequency of the speed sensor signal is 180 times that of the terminal voltage. Figure 9 shows that, under load conditions, by extracting the sinusoidal tabular data in the ROM, the CPU controls the DA converter to output the voltage reference, which has the same frequency and phase as the generator terminal voltage.

5.3. Optimal back-stepping robust adaptive excitation control simulation of the military moving power station

Case 1 (when $\varepsilon_i = 0$)
The 50% rated load is increased at 0.53 s. When the PID control is adopted, the curves of the state variables of the MMPS are shown in Figure 10(a).

When $m_1 = m_2 = m_3 = 3$, $\rho = 1$, $Q = \mathrm{I}$, $R = 1$ and the OBRAEC is adopted, the curves of the state variables of the generator are shown in Figure 10(b).

As shown in Figure 10(a) and (b), when the load is increased suddenly, OBRAEC can improve the convergence rate of the state variables compared with PID control. Because the damp constant D is uncertain, the OBRAEC can increase the robust performance of the uncertain excitation system effectively, as shown in Figure 10(b).

When $m_1 = 4$, $m_2 = 5$, $m_3 = 3$, $\rho = 1$, $\boldsymbol{Q} = \mathrm{diag}[9, 2, 1]$, $R = 1$ and the OBRAEC is adopted, the curves of the state variables are shown in Figure 11.

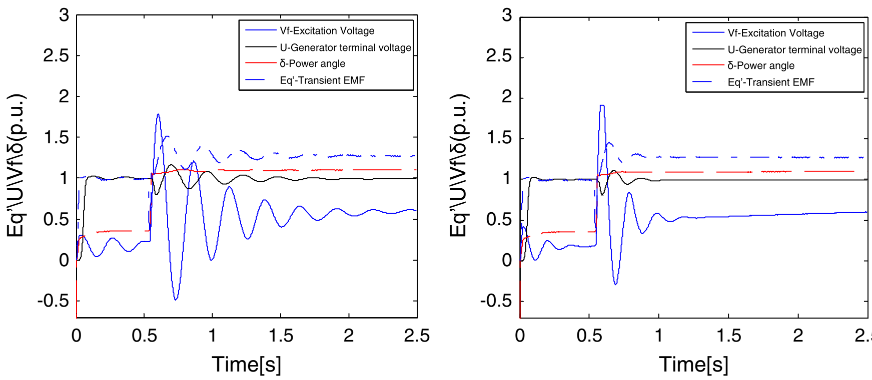

(a) PID control (b) OBRAEC control

Figure 10. Comparison between the proportional integral derivative control and the optimal back-stepping robust adaptive excitation control.

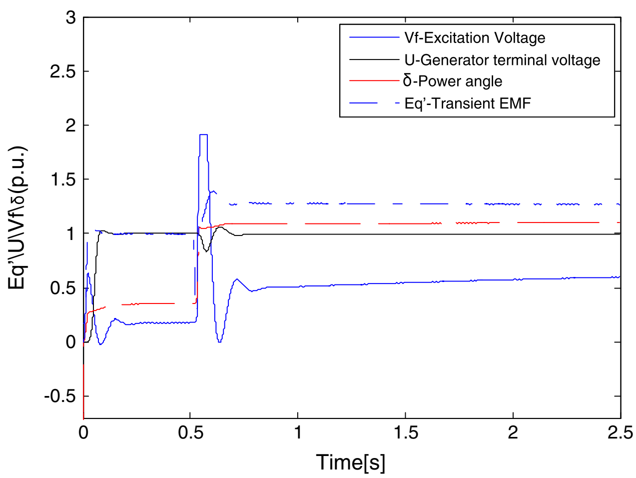

Figure 11. Curves of the generator state variables by optimal back-stepping robust adaptive excitation control.

As shown in Figures 10(b) and 11, when the values of $\boldsymbol{Q}$ and $\boldsymbol{R}$ change, the convergence rate of the state variables can be improved. The $\boldsymbol{J} = \frac{1}{2}\int_0^\infty \left(q_1(\delta-\delta_0)^2 + q_2(\omega-\omega_0)^2 + q_3\dot{\omega}^2 + v^2\right) dt = \boldsymbol{J}_{\min}$ can be realised in the OBRAEC.

Case 2 (when $\varepsilon_i \neq 0$)

When torque and electromagnetic interferences are present in system (1), $y = \boldsymbol{C}\boldsymbol{Z}$, $\boldsymbol{C} = \mathrm{diag}[1, 0.5, 0.2]$, $m_1 = 2$, $\gamma = 1$ and the LMI (54) can be resolved by the function feasp in the MATLAB LMI toolbox. We can obtain $\boldsymbol{P} = \begin{bmatrix} 1.7707 & -0.9579 & 0.2963 \\ -0.9579 & 2.1581 & 0.1932 \\ 0.2963 & 0.1932 & 2.7826 \end{bmatrix}$ and $\boldsymbol{W} = [17.5164 \quad -2.4073 \quad -1.9690]$.

From (39) and (40), the optimal robust control law v_2 and the worst disturbances $\boldsymbol{w}$ are respectively presented as follows:

$$v_2 = 12.9103z_1 + 4.8313z_2 - 2.4179z_3 = 12.9103(\delta-\delta_0) + 4.8313(\omega-\omega_0) - 2.4179\dot{\omega} \quad (56)$$

$$\boldsymbol{w} = \begin{bmatrix} 0.2395 & -0.5395 & -0.0483 \\ 0.0741 & 0.0483 & 0.6956 \end{bmatrix} \begin{bmatrix} \delta-\delta_0 \\ \omega-\omega_0 \\ \dot{\omega} \end{bmatrix}. \quad (57)$$

DOI: 10.1002/rnc

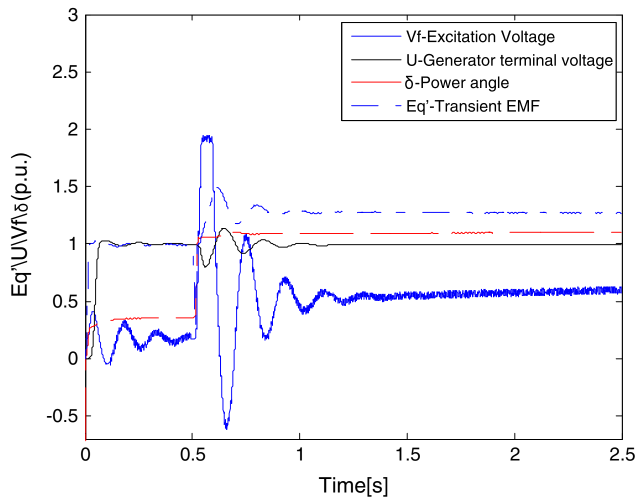

Figure 12. The curves of the state variables by optimal back-stepping robust adaptive excitation control.

Substituting (56) into (55) and (48), we can obtain the control input u. The adaptive law is expressed by (49). The curves of the state variables are shown in Figure 12.

As shown in Figure 12, the OBRAEC can suppress the disturbance, stabilise the excitation system and is adaptive to uncertain parameters. In Figure 12, the curve of V_f is unstable because the excitation input is composed of the noise.

6. CONCLUSION

A new recursive method for nonlinear robust adaptive control design is proposed in this paper for a class of nonlinear systems that can be transformed into parametric feedback form. Compared with the conventional back-stepping robust adaptive control, the new method is robust to external disturbance and adaptive to uncertain parameters. Moreover, the method can realise optimal control and optimal L2 gain disturbance attenuation. Based on this new method, the AC tracking OBRAEC of the MMPS is investigated. To realise the OBRAEC on all operating points, the values of the state variables on different operating points are obtained using EKF tracking estimation and synchronous calculation. The electrical network of the MMPS has limited capacity and is easily affected by the weapon equipment, such that the generator terminal voltage (GTV) fluctuates strongly. The sampling speed of the GTV affects the control speed. In this paper, the GTV is sampled by the AC tracking comparison with voltage reference. The simulation results show that the controller can effectively stabilise the system, be adaptive to uncertain parameters and realise optimal disturbance attenuation.

ACKNOWLEDGEMENTS

This work is supported by the Science Foundation of Mechanical Engineering College (Grant No. YJJ10031 and YJJXM12046).

REFERENCES

1. Zhifeng G, Changqing Z, Tianzhang S, Chuanchuan W, Qiaojing A. Study on the AC tracking excitation based on the sensor-less air-gap field oriented technology. *Electric Power Automation Equipment* 2011; **10**(3):52–56.
2. Yan C, Venayagamoorthy GK, Corzine K. Hardware implementation of an AIS-based optimal excitation controller for an electric ship. *IEEE Transactions on Industry Applications* 2011; **47**(2):1060–1070.
3. Huang ML. Simulation research on H_∞ voltage regulator for synchronous generator of a ship power station. *Journal of Harbin Engineering University* 2004; **25**(2):162–166.

4. Park S, Lee S, Lee S, Yu J, Lee S, Wona C. Output voltage control of a synchronous generator for ships using compound type digital AVR. *31st International Telecommunications Energy Conference*, Incheon, Korea, 2009; 1–8.
5. Arcidiacono V, Castellan S, Menis R, Sulligoi G. Integrated voltage and reactive power control for all electric ship power systems. *International Symposium on Power Electronics, Electrical Drives, Automation and Motion*, Taonnina, Italy, 2006; 878–882.
6. Arcidiacono V, Menis R, Sulligoi G. Improving power quality in all electric ships using a voltage and VAR integrated regulator. *2007 IEEE Electric Ship Technologies Symposium*, Arlington, VA, USA, 2007; 322–327.
7. Deqiang G, Zhihua Q, Hongzhi C. Multi-machine power system excitation control design via theories of feedback linearization control and nonlinear robust control. *International Journal of Systems Science* 2000; **31**(4):519–527.
8. Cong L, Wang Y, Hill DJ. Coordinated control design of generator excitation and SVC for transient stability and voltage regulation enhancement of multi-machine power systems. *International Journal of Robust and Nonlinear Control* 2004; **14**(9):789–805.
9. Lu Q, Sun Y, Xu Z, Mochizuki T. Decentralized nonlinear optimal excitation control. *IEEE Transactions on Power Systems* 1996; **11**(4):1957–1962.
10. Hiyama T, Ueki Y, Andou H. Integrated fuzzy logic generator controller for stability enhancement. *IEEE Transactions on Energy Conversion* 1997; **12**(4):400–406.
11. Hsu Y, Chen L. Tuning of power system stabilizers using an artificial neural network. *Transactions on Energy Conversion* 1991; **6**(4):612–619.
12. Guo Y, Hill DJ, Wang Y. Global transient stability and voltage regulation for power systems. *IEEE Transactions on Power Systems* 2001; **16**(4):678–688.
13. Chapman JW, Ilic MD, King CA, Eng L, Kaufman H. Stabilizing a multi-machine power system via decentralized feedback linearizing excitation control. *IEEE Transactions on Power Systems* 1993; **8**(3):830–839.
14. Hao J, Chen C, Shi L, Wang J. Nonlinear decentralized disturbance attenuation excitation control for power systems with nonlinear loads based on the Hamiltonian theory. *IEEE Transactions on Energy Conversion* 2007; **22**(2):316–324.
15. Wang YZ, Li CW, Cheng DZ. New approaches to generalized Hamiltonian realization of autonomous nonlinear systems. *Science in China (Series F)* 2003; **46**(6):431–444.
16. Loukianov AG, Canedo JM, Fridman LM, Soto-Cota A. High-order block sliding-mode controller for a synchronous generator with an exciter system. *IEEE Transactions on Industrial Electronics* 2011; **58**(1):337–347.
17. Lu Q, Mei S, Hul W. Nonlinear decentralized disturbance attenuation excitation control via new recursive design for multi machine power systems. *IEEE Transactions on Power Systems* 2001; **16**(4):729–736.
18. Polycarpou MM, Ioannou PA. A robust adaptive nonlinear control design. *Automatica* 1996; **32**(3):423–427.
19. Marino R, Tomei P. Robust adaptive state-feedback tracking for nonlinear systems. *IEEE Transactions on Automatic Control* 1998; **43**(1):84–89.
20. Jiang ZP, Hill DJ. A robust adaptive back-stepping scheme for nonlinear systems with unmodeled dynamics. *IEEE Transactions on Automatic Control* 1999; **44**(9):1705–1711.
21. Wang K, Xin H, Gan D, Ni Y. Nonlinear robust adaptive excitation controller design in power systems based on a new back-stepping method. *IET Control Theory and Applications* 2010; **4**(12):2947–2957.
22. Cai Z, de Queiroz MS, Dawson DM. Robust adaptive asymptotic tracking of nonlinear systems with additive disturbance. *IEEE Transactions on Automatic Control* 2006; **51**(3):524–529.
23. Gao F, de Queiroz MS, Dawson DM. A new tuning function-based robust adaptive controller for parametric strict-feedback systems. *46th IEEE Conference on Decision and Control*, 2007; 3543–3548.

DOI: 10.1002/rnc